Research Article

Yue Yu*

Research on the performance of a novel type of cemented filler material for coal mine opening and filling

https://doi.org/10.1515/nleng-2025-0113
received November 26, 2024; accepted March 3, 2025

Abstract: In this study, Inner Mongolia Chahasu Coal Mine is considered as the research object and new type of cemented filling material is developed based on gangue, fly ash, and cement. The aim is to systematically optimize its performance and investigate the influencing factors to improve the proportion of cemented filling materials used in the coal mine filling and mining process. Thus, the study seeks to reduce production costs and enhance the utilization rate of solid waste. In the literature, various studies have focused on optimizing the performance of cemented filling materials, particularly in terms of reducing environmental impact and improving cost-effectiveness. Research abroad has made significant progress in optimizing filling materials under specific geological conditions, such as varying mineral compositions and groundwater influences. However, the challenge remains in balancing the physical properties like compressive strength, flowability, and durability with the efficient use of industrial byproducts such as fly ash and gangue. Studies also indicate that while cemented filling materials have been extensively studied for their strength properties, the interaction effects of multiple factors, particularly in complex mining environments, are not well understood. In contrast, domestic studies primarily focus on the basic performance of filling materials under less variable geological conditions, with limited emphasis on how environmental complexities impact the optimization process. Furthermore, many studies do not fully address the role of gangue particle size and fly ash in improving the environmental sustainability and cost-effectiveness of filling materials. To fill this gap, this study combines the response surface methodology with optimization of the gangue particle size gradation to create a response model between cement, fly ash, solid content, and the filler body's compressive strength. According to the test results, the filling materials' strength and flowability were maximized when the grading factor of the gangue particle size was set at n = 0.5. A Box–Behnken experimental design was then used to examine the influence patterns of cement, fly ash, and solid content on the filling body's strength at the early (3 days), middle (7 days), and late (28 days) stages, focusing on both single-factor and multi-factor interactions. The study found that the primary determinants of strength were the cement mass fraction and solid mass fraction, with fly ash's contribution becoming more significant in the later stages of curing. The optimized ratios not only met the filling strength requirements but also significantly reduced cement usage and increased the utilization rate of fly ash, demonstrating the potential for both cost reduction and effective resource usage of solid waste.

Keywords: coal gangue, fly ash, cementitious filling material, particle size grading, response surface analysis, strength optimization, coal mining

1 Introduction

The coal mining industry faces the dual challenges of efficient mining and environmental conservation due to the ongoing rise in energy demand and growing ecological preservation consciousness [1]. Surface subsidence, ecological harm, and the buildup of solid waste in the mining area as a result of overexploitation have all become more significant issues in the traditional coal mining process. These issues not only jeopardize the long-term viability of the local ecological environment but also have an impact on the region's economic and social advantages. Fill mining technology has evolved and is progressively becoming a significant development path of green mining technology in an effort to resolve the aforementioned inconsistencies [2,3].

The continuous mining and filling roadway-type cemented filling coal mining method is typically used in the coal mining area. By instantly replenishing the mining area, this method not only efficiently addresses the issue of surface collapse but

* **Corresponding author: Yue Yu,** School of Civil Engineering, Liaodong University, Dandong, 118003, China, e-mail: yuyue@liaodongu.edu.cn

also increases coal mining efficiency [4]. Though the usage rate of industrial wastes like fly ash is less than 15%, the current filling materials contain a large amount of cement (more than 12%), which drives up material costs and prevents the effective removal of solid wastes. Thus, the development of innovative cementitious filling materials with superior performance and affordable prices is very necessary [5].

Fluidity, water secretion rate, and strength are the primary indications of the performance of cemented filler materials, which are typically made of cement, fly ash, gangue, and water [6]. Researchers, both domestically and internationally, have advanced cementitious filling material optimization and performance improvement in recent years. Modifying the material ratio, improving aggregate grading, and adding additional additives are examples of common improvement techniques. For instance, increasing the amount of fly ash mixed in to replace some of the cement can lower costs without sacrificing strength; modifying the gangue particle size grading can increase the filler body's strength and fluidity [7].

However, the current cementitious materials are not very adaptable to complex mining settings; in particular, the material performance is difficult to ensure in extreme environments or unusual engineering needs. The effective use of industrial wastes like fly ash and gangue has not yet been achieved, and resource waste and environmental protection pressures coexist [8]. There is a significant gap between the experimental design and real-world application since some research in the material optimization process is not systematic and does not fully take into account the interplay of many components [9].

Therefore, in order to solve the aforementioned issues, it is imperative to develop novel materials that satisfy a variety of performance requirements as well as to build the theoretical underpinnings and methodological framework for maximizing the performance of cemented filler materials through methodical research.

Based on the unique engineering requirements of coal mining areas, this study seeks to create a cementitious filling material that is both economical and high-performing by optimizing the proportions of cement, fly ash, and gangue. The goal is to ensure that the filling body is strong and fluid, minimize the amount of cement, and enhance the amount of fly ash and gangue that is mixed in order to achieve the most efficient use of waste resources [10]. The ideal gradation and proportion are identified to enhance the overall performance of filler materials by examining the effects of gangue particle size gradation and material proportion on strength and fluidity. The response model of material performance and proportioning parameters is established using contemporary optimization techniques like the response surface method (RSM), and the optimization effect is confirmed from both theoretical and practical viewpoints [11,12].

Despite the wide range of potential applications for cementitious filler materials, there are still certain obstacles to overcome in their implementation and promotion. First, a number of performance metrics, including the potential conflict among strength, fluidity, and water secretion rate, must be balanced while optimizing the percentage of filling ingredients. Second, material development must have a significant capacity for environmental adaptation due to the complicated and varied geological conditions found in various mining sites. This study uses a methodical design of experiments strategy to address these issues, integrating mathematical modeling and physical testing to maximize the filling material performance and proportioning.

2 Project overview

2.1 An outline of the functioning face

The Chahasu Coal Mine in Inner Mongolia adopts continuous highway-type mining and filling-cemented coal mining technology for its operations. The scope of the infill mining area spans 200 m along the strike direction and 500 m along the coal seam inclination direction. Within this mining region, four infill workings are planned: 301, 302, 303, and 304. Each of these workings extends 500 m in the direction of the coal seam's inclination and 50 m along the strike direction.

Following the completion of back mining in the 301 workings, the mining process for the 302 workings commenced. The mining operations are organized and coordinated in phases, with a sequential approach to the filling mining in each of the designated workings. The mining plan ensures that the infill mining activities are carried out in a manner that maximizes resource extraction while minimizing operational risks.

The configuration of the mining operations, as depicted in Figure 1, outlines the spatial arrangement and sequence of the workings. This configuration has been designed to optimize efficiency and ensure safety during the mining process. The systematic approach to filling and back mining allows for improved stability of the coal seam and reduces the potential for surface subsidence or other negative impacts on the surrounding environment.

2.2 Backfilling process

In total, there are 90 branches, with each branch of the 302 face measuring 5 m in width and 50 m in length. "Mining in

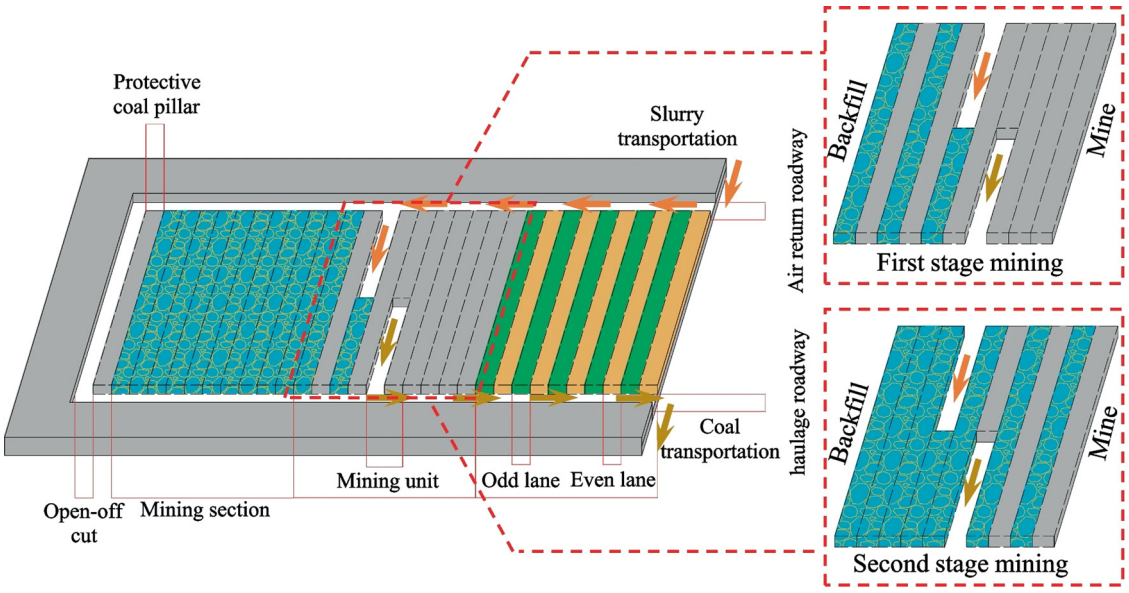

Figure 1: Chahasu Coal Mine's working face 302 arrangement.

three intervals" is the mining method, and "three strong and one weak" is the filling mode. In particular, there is a coal pillar (filling body) spaced every 15 m. The pillar is filled on schedule once a 5 m wide branch has been mined; the remaining branches are mined back and filled in accordance with the predetermined order after the filling body reaches the appropriate strength. The coal pillars of the 302 face are spaced 20 m apart, with four branch lanes in each group. The backmining sequence, using the first group as an example, is carried out in the following order: 1 → 3 → 2 → 4, with high strength filling the first, third, and second branch lanes and low strength filling the fourth. Figure 2 illustrates the filling procedure.

The filling materials for the back mined and filled 301 and 302 workings have a cement content of over 12% and a fly ash component of less than 15%. Despite lowering filling costs, this ratio does not efficiently use the solid waste generated by coal mines. As a result, in order to ensure the strength of the filling body and the slurry conveying performance, the ratio of filling materials must be optimized to use more fly ash and less cement.

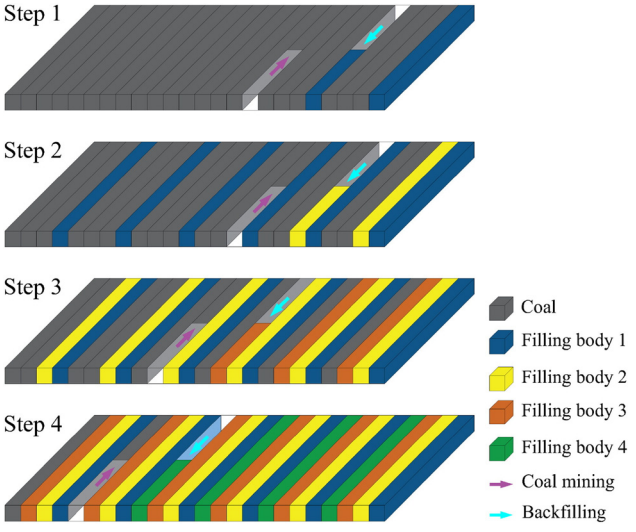

Figure 2: Filling process.

3 Analysis of gangue grading and test content

3.1 Examining the procedure and content

Coal gangue is utilized as an aggregate, fly ash serves as an auxiliary material, and cement is employed as a binding agent, with mine water mixed to form a homogeneous slurry at a specific mass fraction. This slurry is then transported to the filling face for the mining process. The fly ash used in the formulation is sourced from the Bulian power station, while P.O42.5 ordinary silicate cement is selected as the cementing component to ensure strong bonding properties. The coal gangue, extracted from the Tsahasu coal mine in Inner Mongolia, provides the bulk material for the slurry [13].

The combination of these materials – coal gangue, fly ash, and cement – ensures both the mechanical strength

and stability of the filling material, which is crucial for maintaining the structural integrity of the mined area. The use of mine water facilitates the proper consistency and flow of the slurry, making it suitable for filling voids in the mining process. Additionally, the incorporation of fly ash not only improves the workability and performance of the slurry but also contributes to sustainability by utilizing industrial by-products, thus reducing environmental impact. The use of local materials such as coal gangue from the Tsahasu mine further enhances the sustainability of the mining operation, minimizing transportation costs and reducing the carbon footprint associated with the material procurement process.

This carefully optimized slurry formulation plays a vital role in supporting safe and efficient mining operations, ensuring both environmental and operational benefits.

In order to optimize the proportion of filling materials, the gangue particle size was first graded and optimized. Then, the influence law of cement, fly ash, and solid content on the filling body's strength was examined using the RSM. The optimized slurry is evaluated for slump and water secretion rate in order to ensure that the filling body's strength satisfies the required level. As part of the optimization process, solid ingredients like cement, fly ash, and gangue are added to the mixer and thoroughly mixed. Mine water is then added, and the mixture is continued until the slurry is homogenous [14]. After initial hardening, the slurry was poured into 80 mm × 80 mm × 100 mm molds, scraped flat, and vibrated before being demolded and kept in a maintenance room with a minimum humidity of 90% and a temperature of 20°C. Following 3, 7, and 21 days of curing, the specimen blocks were subjected to a uniaxial compression test using a Changchun YAD-2000 electrohydraulic servo press in order to determine the relevant strength data. The test was carried out using a loading rate of 0.5 mm/min in the displacement control mode.

After choosing the material proportion that meets the downhole filling strength criteria, the slump and water secretion rate test is carried out. In the slump test, the slurry was loaded into the slump cylinder three times and lifted at a steady speed after each filling, and the height difference between the top of the slurry and the bottom of the slump cylinder was measured with a steel ruler to

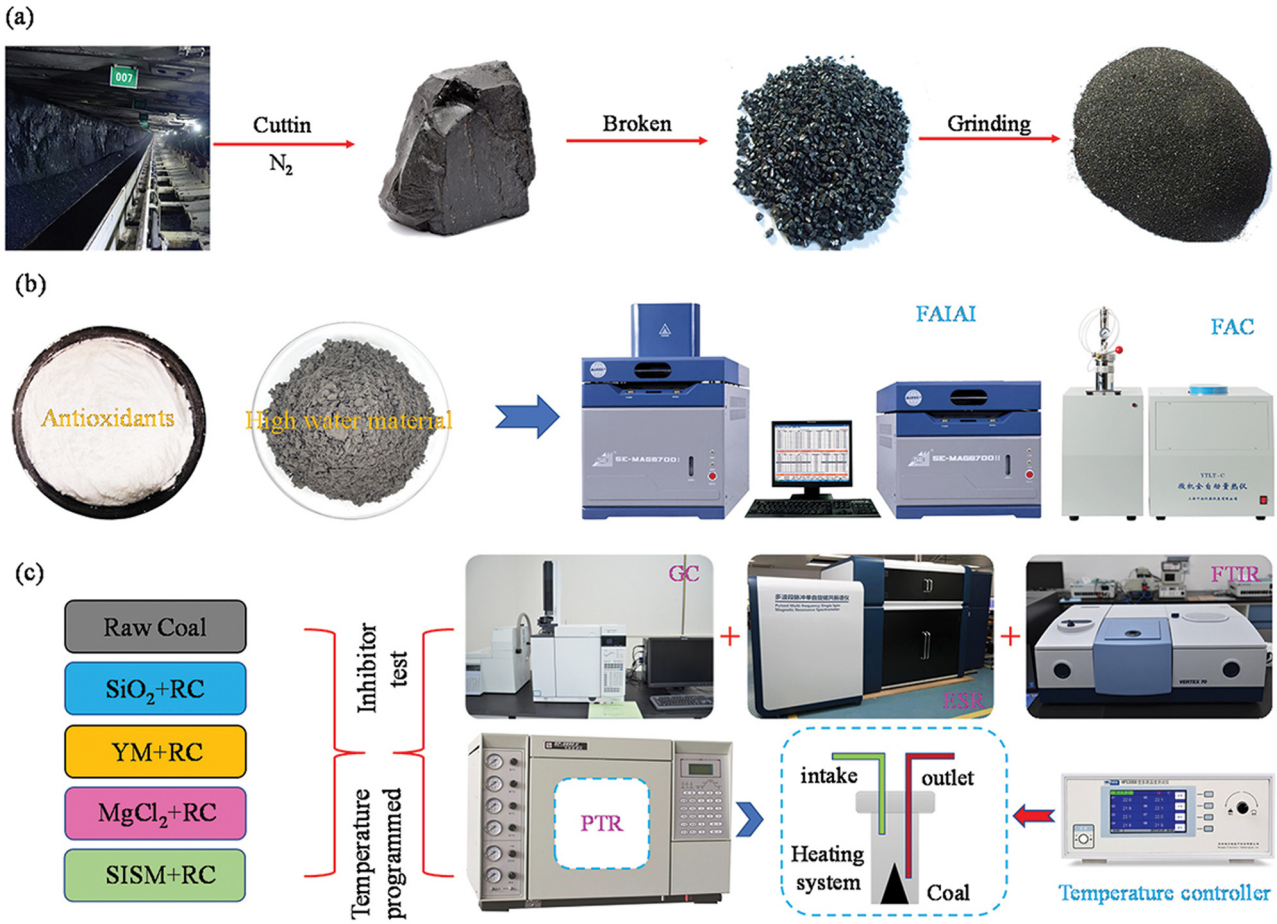

Figure 3: Ratio optimization experimentation. (a) Coal sample preparation. (b) Optimization of SISM ratio. (c) Inhibitor performance test.

Table 1: Gangue size grading scheme

Particle size range of gangue (mm)	Percentage of particle size under various grading coefficients					
	***N* = 0.1**	***N* = 0.2**	***N* = 0.3**	***N* = 0.4**	***N* = 0.5**	**Configuration that is natively incorporated**
10–15	8	10	12	16	18	15
5–10	11	13	17	19	21	20
<5	61	58	54	52	47	52

calculate the slump value [15]. The slurry was then inserted and uniformly pounded with a tamping rod. In order to perform the lactation rate test, the slurry was loaded into a lactation rate cylinder with a lubricated inner wall. The cylinder and the slurry were then weighed, and every 15 min, the water secreted from the slurry was pipetted into the cylinder until it stopped or became trace. The percentage of the slurry's total mass and secretion was then used to compute the lactation rate. The exact flow of the test is shown in Figure 3.

3.2 Analysis of gangue grading

Figure 3: Experiments to optimize the ratio of the cemented filling material.

Figure 3 shows the experiments to optimize the ratio of the cemented filling material. The strength of the filler body is significantly impacted by the gangue particle size grading. Taiwanese theory states that the native grading is utilized as a control group, and the gangue particle size grading coefficients for the 0–5, 5–10, and 10–15 mm gangue particle size grading groups are 0.1–0.5. Table 1 displays the gangue particle size grading methodology for the 0.7, 0–5, 5–10, and 10–15 mm gangue particle size grading groups, with the native grading serving as the control group. The cement/fly ash/gangue/water ratio is 12:18:50:20, and the mass fraction of the cemented filler body is kept at 75%. Figure 4 illustrates the strength of the filling body and the fluidity of the filling slurry under various grading coefficients.

As the gradation factor n increases, the slump of the filled slurry tends to increase and then decrease, as shown in Figure 4a. When n = 0.5, the mobility reaches its maximum. This is due to the fact that when n increases, the slurry's viscosity decreases and its slump increases as its coarse particles increase and its microscopic particles decrease. However, the slurry's fluidity and slump decrease as n increases because the high coarse particle content increases the sliding friction resistance between large particles. Additionally, as n increases, the slurry's water secretion rate continues to increase. The slump of the slurry increases with increasing n, and the slump of the slurry increases with increasing n.

The filled specimens' uniaxial compressive strength at varying ages exhibits a tendency to grow and subsequently decrease as n increases, as shown in Figure 4b. Compared to other gradation factors, the specimens at n = 0.4 and n = 0.5 had a substantially higher uniaxial compressive strength. The specimens' compressive strengths at n = 0.4 and n = 0.5 are noticeably greater than those of the other gradation factors. This is because the grading between the particles

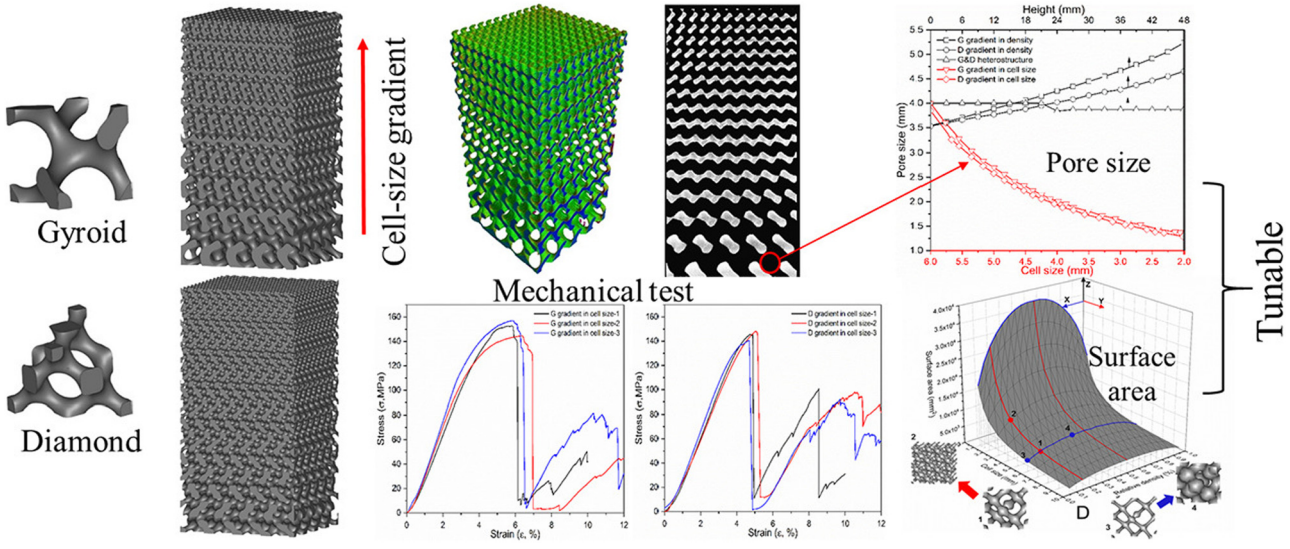

Figure 4: Filling material performance results with varying grading coefficients.

is more uniform when n is in the moderate range (n = 0.4–0.5). On the one hand, the fine particles can fill the pores between the coarse particles; on the other hand, the fine particle content is lower than with a smaller n, and the hydration products can better encapsulate the gangue particles, increasing the filler's strength. When n = 0.5 is combined with the compressive strength and mobility experimental data, the gangue grading reaches its optimal state.

Both of them are greater than 0.5 for the primary grade when the gangue content of particle size n = 0.1 mm is 80%; n = 0.5 indicates a higher proportion of coarse particles. To bring the grading coefficient close to n = 0.5, the fine gangue content should be suitably raised. The compressive strengths of the test pieces on days 3, 7, and 21, under native grading conditions, were 0.5, 2.5, and 6.5 MPa, respectively. These values were less than the compressive strengths at each age when n = 0.5.

4 Optimizing material proportioning using the RSM-BBD approach

4.1 Experimental design and results

Numerous factors influence the performance of the cemented filling materials. To examine the impact of ongoing changes and the interplay of various factors, a response model of the uniaxial compressive strength of cemented filler with various factors is created using RSM design software Design-Expert [16]. From the results above, the gangue grading coefficient, n = 0.5, was calculated. Three major influencing factors were chosen based on the Box–Behnken design (BBD) experimental design: cement mass fraction X_1 (5–10%), fly ash mass fraction X_2 (11–15%), and solid mass fraction X_3 (16–20%). This was because the fly ash mass fraction was less than 15%, and the cement mass fraction of the original cemented filling material exceeded 12%. Three major influencing elements were chosen based on the BBD experimental design: solids mass fraction X_3 (30–35%), fly ash mass fraction X_2 (20–25%), and cement mass fraction X_1 (5–15%).

The strengths predicted by the response surface analysis were expressed as Y_1', Y_2', Y_3', while the measured strengths of the filled body on days 3, 7, and 21 were expressed as Y_1, Y_2, Y_3. The BBD approach was used to design 13 test groups, and Table 2 displays the findings of the RSM-BBD test design and analysis.

By using the Design Expert software to statistically analyze the test data in Table 2, the following response surface functions of the filler's compressive strength on days 3, 7, and 21 were obtained:

$$Y_1' = 82.23 + 1.12X_1 + 1.10X_2 - 2.50X_3 - 0.001X_1X_2 - 0.006X_1X_3 - 0.004X_2X_3 - 0.01X_1^2 - 0.02X_2^2 + 0.02X_3^2, \quad (1)$$

$$Y_2' = -350.24 - 1.32X_1 + 8.68X_2 + 6.45X_3 - 0.01X_1X_2 + 0.03X_1X_3 - 0.05X_2X_3 - 0.02X_1^2 - 0.10X_2^2 - 0.03X_3^2, \quad (2)$$

$$Y_3' = -652.58 + 0.25X_1 + 4.65X_2 + 14.32X_3 - 0.05X_1X_2 + 0.04X_1X_3 + 0.06X_2X_3 - 0.16X_1^2 - 0.25X_2^2 - 0.08X_3^2. \quad (3)$$

By choosing the values of any one of the three factors, the Design Expert software's simulation results can be used to determine the compressive strength results under the relevant conditions. This makes it simple to examine the effects of a single factor or the interaction of several factors under various conditions.

4.2 Reliability investigation of the RSM regression model

The analysis of variance (ANOVA) of the filler block's compressive strength on days 3, 7, and 21 was performed using Design Expert software to assess the accuracy and precision of the response surface regression results. The results

Table 2: Results of the RSM-BBD experimental design and analysis

Group	X_1 (%)	X_2 (%)	X_3 (%)	3D strength (MPa)			7D strength (MPa)			21D strength (MPa)		
				Y_1	Y_1'	Relative error (%)	Y_2	Y_2'	Relative error (%)	Y_3	Y_3'	Relative error (%)
1	6	8	75	0.25	0.30	−3.24	1.22	0	0.25	2.53	2.84	−1.59
2	10	12	75	0.82	0.84	2.25	2.55	2.75	5.23	6.36	6.25	−1.57
3	6	8	75	0.35	0.32	−5.57	1.68	1.45	−8.52	3.23	3.55	2.56
4	10	14	72	0.82	0.84	1.16	2.25	2.32	0.32	6.45	6.44	2.68
5	14	19	80	0.22	0.21	−4.15	1.14	1.23	6.28	2.24	2.31	3.54

Table 3: ANOVA of the regression model for compressive strength

Source of variance	Sum of squares (MPa^2)			Variance (MPa^2)			*F* value			*P* value		
	Y_1	Y_2	Y_3	Y_1	Y_2	Y_3	Y_1	Y_2	Y_3	Y_1	Y_2	Y_3
Regression model	0.856	6.254	56.24	0.089	0.725	6.325	115.6	45.89	266.52	0.001	0.001	0.001
X_1	0.584	2.654	20.365	0.587	2.621	23.45	652.14	174.88	858.21	0.001	0.001	0.001
X_2	0.004	0.0125	0.9871	0.004	0.0125	0.9857	4.25	0.89	38.56	0.074	0.365	0.004
X_3	0.234	2.565	24.578	2.565	24.578	287.65	174.52	257.65	1016.32	0.001	0.001	0.001
X_1X_2	0.002	0.025	0.235	0.002	0.064	0.254	0.25	4.32	9.4	0.625	0.074	0.0147
X_1X_3	0.004	0.0784	0.268	0.005	0.0784	0.268	5.24	5.26	12.45	0.078	0.056	0.0098
X_2X_3	0.002	2.958	0.457	0.003	0.289	0.4201	18.5616.25	15.25	16.32	0.132	0.003	0.004
X_1^2	0.015	0.046	2.451	0.015	0.046	2.454	15.68	3.25	100.32	0.05	0.124	0.0001
X_2^2	0.018	0.741	5.624	0.015	0.784	5.654	20.36	48.56	22.54	265.47	0.002	0.0001
X_3^2	0.025	0.0987	0.658	0.025	0.096	0.684	25.68	6.52	27.65	0.001	0.047	0.0012

of this analysis are summarized in Table 3. To further validate the predictive power of the model, Figure 5 presents a scatter plot comparing the measured compressive strength values of the filling block on days 3, 7, and 21 with the predicted values generated by the model. In this plot, the measured values are plotted on the horizontal axis,

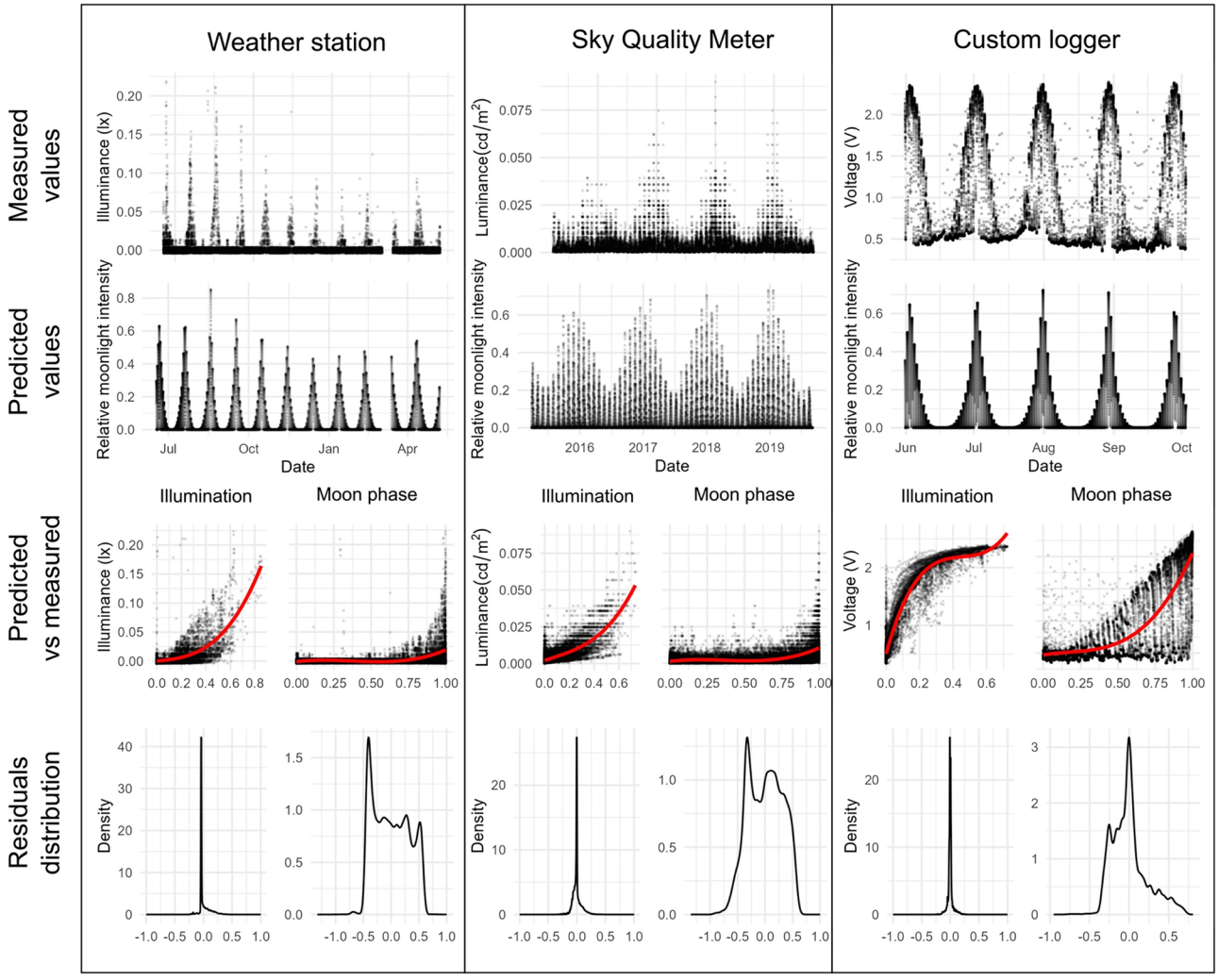

Figure 5: Comparison of the predicted and measured intensity values.

while the predicted values are plotted on the vertical axis, allowing for a direct comparison of the two sets of data.

This graphical representation serves to highlight the correlation between the experimental data and the predicted outcomes, providing insights into the model's predictive accuracy. Ideally, the data points should closely align with the 45-degree diagonal line, which would indicate a high degree of agreement between the observed and predicted compressive strength values. Any significant deviation from this line could suggest areas for further model refinement or indicate underlying factors not fully captured by the current model. By visualizing this comparison, the effectiveness of the response surface regression model can be more thoroughly evaluated.

The ANOVA results in Table 3 demonstrate that the regression model has excellent statistical significance and predictive power, with the F values for the filler strength at the three ages being much larger than the critical value [17]. The accuracy and dependability of the compressive strength fitting model of the filling body at three ages are further confirmed by the fact that the scatter points of the measured and predicted values are near the straight line of *XY* and that the relative errors between the predicted and measured values are kept within ±10% when Table 2 and Figure 5 are combined. This model can also be used to predict and analyze test results.

Additional examination of Table 3 reveals that a two-factor interaction has a considerable impact on the filler's strength in addition to a single factor. At 3 days of age, the strength was significantly impacted by the cement mass fraction, solid mass fraction, and cement–solid mass fraction interactions, but the fly ash mass fraction interaction was not significant, suggesting that fly ash had a minimal impact on early strength. Strength was significantly impacted by cement mass fraction, solids mass fraction, and fly ash interaction with solids mass fraction after 7 days of aging. Strength was significantly impacted at 21 days of age by the cement mass fraction, fly ash mass fraction, solid mass fraction, and the combination of all three.

The cement mass fraction and solid mass fraction were consistently the most important influencing factors on the filler's strength at all ages, according to the significance factor analysis mentioned above. In the late maintenance phase, fly ash gradually discloses its volcanic ash qualities, increasing the filling body's strength. The fly ash mass fraction has a minor impact on the early strength (3 days), but it plays a major role in the late strength (21 days).

4.3 Examination of test findings

4.3.1 Single-factor effect analysis using the RSM model

RSM has the advantage of properly predicting the response index results for any change value within each factor's range of variation. To examine the impact of a single factor, cement mass fraction X_1, fly ash mass fraction X_2, and solids mass fraction X_3, on the strength, five values of each factor can be selected within the range of fluctuation, as illustrated in Figure 6. Figure 6a displays the cement mass fraction X_1 results on strength when X_2 = 15% and X_3 = 75%; Figure 6b displays the fly ash mass fraction X_2 results on strength when X_1 = 10% and X_2 = 16%; and Figure 6c displays the solid mass fraction X_3 results on strength when X_1 = 10% and X_2 = 16%.

Figure 6a makes it clear that cement significantly affects strength throughout the curing phase and that the filler's strength increases with increasing cement mass fraction and curing age. Cement mostly produces calcium silicate (C–S–H), calcium hydroxide (C–H), and alumina (AFt) as hydration products after being hydrated with water. These hydration products fill the interior pores of the filler and wrap the aggregate particles. As the hydration process develops and the cement dose is increased, the filling body's strength significantly

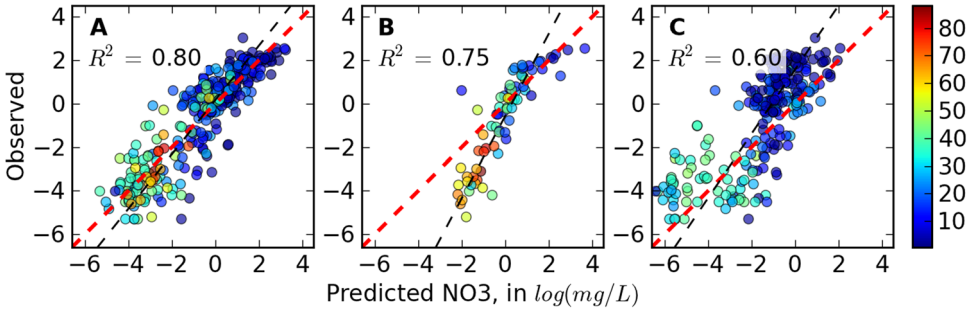

Figure 6: One factor's impact on the filling body's strength. (a) R^2 = 0.80; (b) R^2 = 0.75; and (c) R^2 = 0.60.

increases. With the particles overlapping to create a mesh structure, the resultant hydration products progressively form flocculent agglomerates.

Fly ash mass fraction has a negligible impact on early strength (3–7 days) but a large impact on late strength (21 days), as shown in Figure 6b. Fly ash's microfilling action and volcanic ash activity are the primary factors influencing its strength contribution [18]. Fly ash can fill the pores between gangue as fine particles when the amount is small, which will increase the filling body's strength. However, as the amount of fly ash increases, too many fine particles will cause "oversaturation," which will destroy the ideal particle gradation and result in a decrease in strength. Nevertheless, the volcanic ash activity of fly ash progressively emerges at the conclusion of the 21-day maintenance period and contributes to bonding by mixing with hydration products. The combined effects of volcanic ash activity and the microfilling effect led to a lesser drop in strength at the later stage than at the earlier stage when the mass percentage of fly ash surpassed 18%.

Figure 6c illustrates how the filling body's strength increases steadily as the solid mass fraction and maintenance age rise. A decrease in inter-particle voids, a relative increase in the solid content within the filling body, and the ability of the hydration products to combine with the particles more effectively to form a more compact cluster structure all contributed to the filling body's increased strength.

4.3.2 Impact evaluation of the interplay of RSM parameter

Table 3 shows that the filler's compressive strength is influenced by the substantial interaction of the cement mass fraction, fly ash mass fraction, and solids mass fraction, in addition to their individual effects. Figure 7 illustrates how factor interactions affect the filled bodies' strength at various ages. The strength of the filled body on days 3, 7, and 21 increased as the cement mass fraction and solid mass fraction increased, as shown in Figure 7a–c.

The strength of the filled bodies increased by 0.45 and 0.25 MPa for 3 days, 0.80 and 1.35 MPa for 7 days, and 2.65 and 4.01 MPa for 21 days, respectively, when the cement mass fraction was 8 and 12%, and the solid mass fraction increased from 77 to 81%. In contrast, when the solid mass fraction was 75 and 80%, and the cement mass fraction increased from 8 to 12%, the filled bodies' strengths increased by 0.55 and 0.45 MPa on day 3, 0.82 and 1.35 MPa on day 7, and 2.72 and 3.62 MPa on day 21, respectively. It is evident that the solid mass fraction had a higher impact on the filled bodies' strength on day 21 than the cement mass fraction did on day 3, and the cement mass fraction had a greater impact on the filled bodies' strength on day 3. The strength was higher than the cement mass fraction, and the 7-day strength was similarly impacted by the cement and solid mass fractions, which is in line with the findings in Table 3.

As the other component increased, the impacts of cement and the solids mass fraction on the filled bodies' 3-day strength decreased; however, on days 7 and 21, the strength improvement by both factors progressively increased as the other factor increased. In particular, during the first 3 days of hydration, the cement's specific surface area increases while the filling body's water content drops as a result of an increase in the mass fraction of solids. Although the increase in the mass fraction of solids reduced the pore space of the filling body, which in turn enhanced the strength, the increase in strength was slowed down due to the slowing down of the hydration process. In the case of water reduction, the cement particles were unable to fully contact with the water molecules in a short amount of time, and the hydration reaction process was inhibited, resulting in a slower hydration reaction. The effect of cement and solid mass fraction on the filling body's strength is progressively diminished by the growth of another element because the slowing down of the hydration process is particularly noticeable as cement mass fraction increases.

In the later stages of hydration (days 7 and 21), the strength of the fill increases as cement reacts with water to form more C–S–H, the primary strength-enhancing product. As the solid content increases, particle contact improves, leading to a more compact structure and higher strength. Cement and solid content synergistically enhance the strength.

On day 7 (Figure 7d), the strength increases with solid content, but the effect of fly ash is initially positive and then decreases. On day 21 (Figure 7e), both cement and fly ash influence the strength similarly, with maximum strength occurring at around 18–19% fly ash content. As fly ash and solid content increase, their impact on strength gradually diminishes.

4.4 Mass fraction of the solid phase

The full-scale experiments were carried out according to the above conditions, and the strength, slump, and water secretion on days 7 and 21 were determined for each group, and the results are given in Table 4. The experimental results show that the mass fraction of the slurry and the ash/sand ratio have a significant effect on the workability and strength of the filled slurry. The trend of the solid phase mass fraction on the slurry properties is

shown in Figure 8. It can be seen that the strength on days 7 and 21 increased with the increase of solid phase mass fraction, while the working properties showed the opposite trend. At a 1:4 ratio, the increase of solid fraction from 62 to 75% resulted in 56.9 and 32.5% growth rates of 7 and 21-day strengths and 9.6 and 31.2% reduction in water secretion rate and slumping degree, respectively. The increase in strength is mainly due to the reduction of pore space in the filling body. Correspondingly, an increase in the mass fraction of solids reduces the internal water content of the

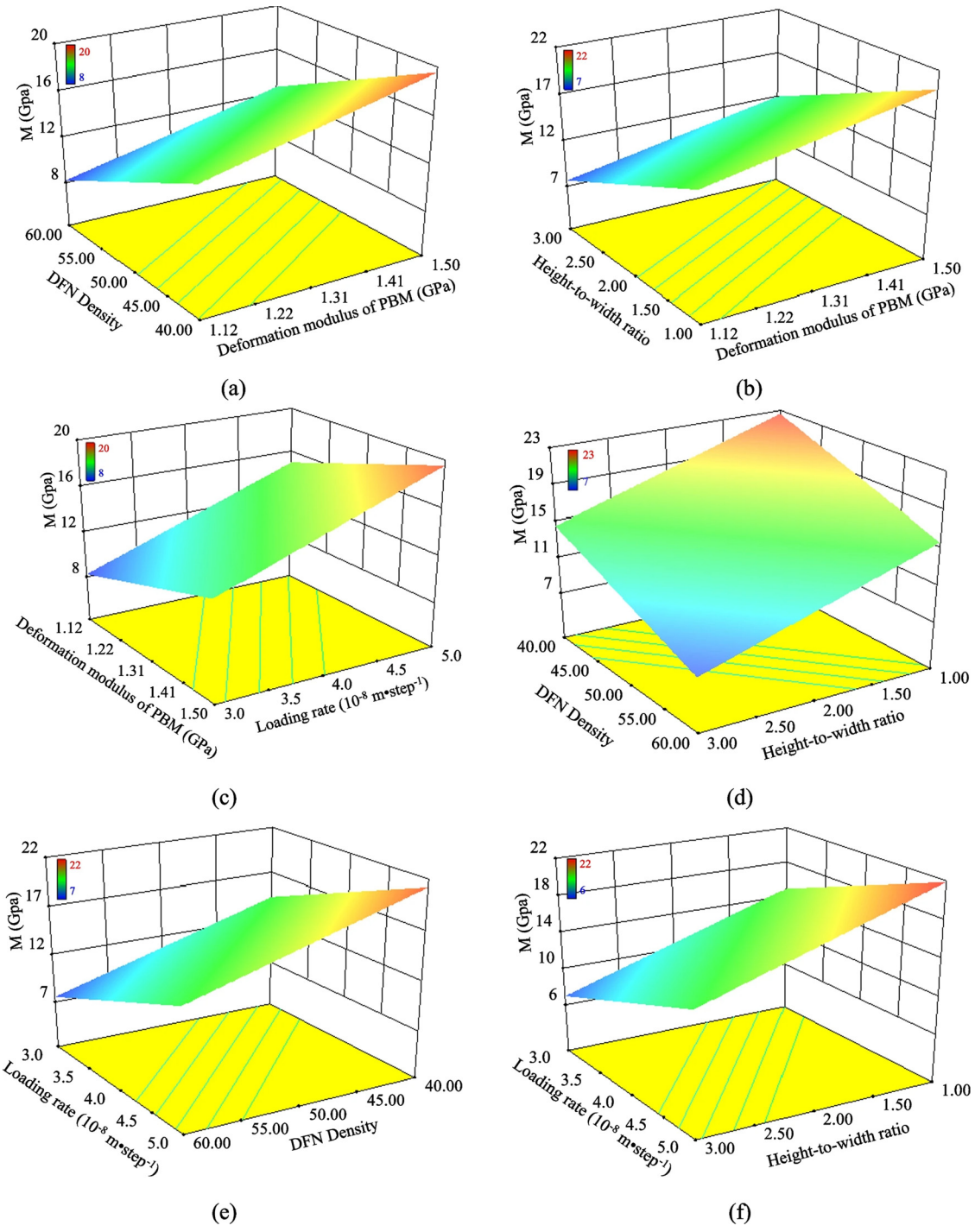

Figure 7: The pattern of factor interactions affects the filling body's strength. (a) The strength of the filled body at 3 days with 0.45 MPa; (b) the strength of the filled body at 3 days with 0.25 MPa; (c) the strength of the filled body at 7 days with 0.80 MPa; (d) the strength of the filled body at 7 days with 1.35 MPa; (e) the strength of the filled body at 21 days with 2.65 MPa; and (f) the strength of the filled body at 21 days with 4.01 MPa.

Table 4: Results of the filling slurry proportioning test

No.	Cement/sand ratio	Solid concentration (%)	7 days	21 days	Slump (cm)	Bleeding rate (%)	Cost
1	1:4	65	1.06	2.54	25.7	9.2	108
2		70	1.32	2.89	26.8	7.4	112
3		75	1.84	3.52	25.6	6.4	114
4	1:6	65	0.84	2.64	25.4	10.8	85
5		70	1.17	2.68	24.8	9.4	85
6		75	0.82	2.72	25.9	9.2	75

slurry, which leads to a decrease in the workability of the slurry. Similarly, the 7 and 21 days strength increases with increasing gray-to-sand ratio, while the workability tends to decrease. This is because an increase in the ash ratio results in more hydration products, which fill and cement the aggregate to form a denser structure and higher strength. However, an increase in the ash/water ratio results in an increase in the number of fine particles in the slurry and an increase in the viscosity of the slurry, which leads to a decrease in the slurry operating characteristics.

Table 4 compares different slurry mixes based on cement/sand ratios, solid concentration, strength, workability (slump), bleeding rate, and cost on days 7 and 21.

The performance data indicate a relationship between the cement/sand ratio and strength development, workability, and cost.

For example, mixtures with a higher solid concentration (*e.g.*, 70 and 75%) generally result in higher compressive strength on days 7 and 21, but they also come with higher costs and varying bleeding rates.

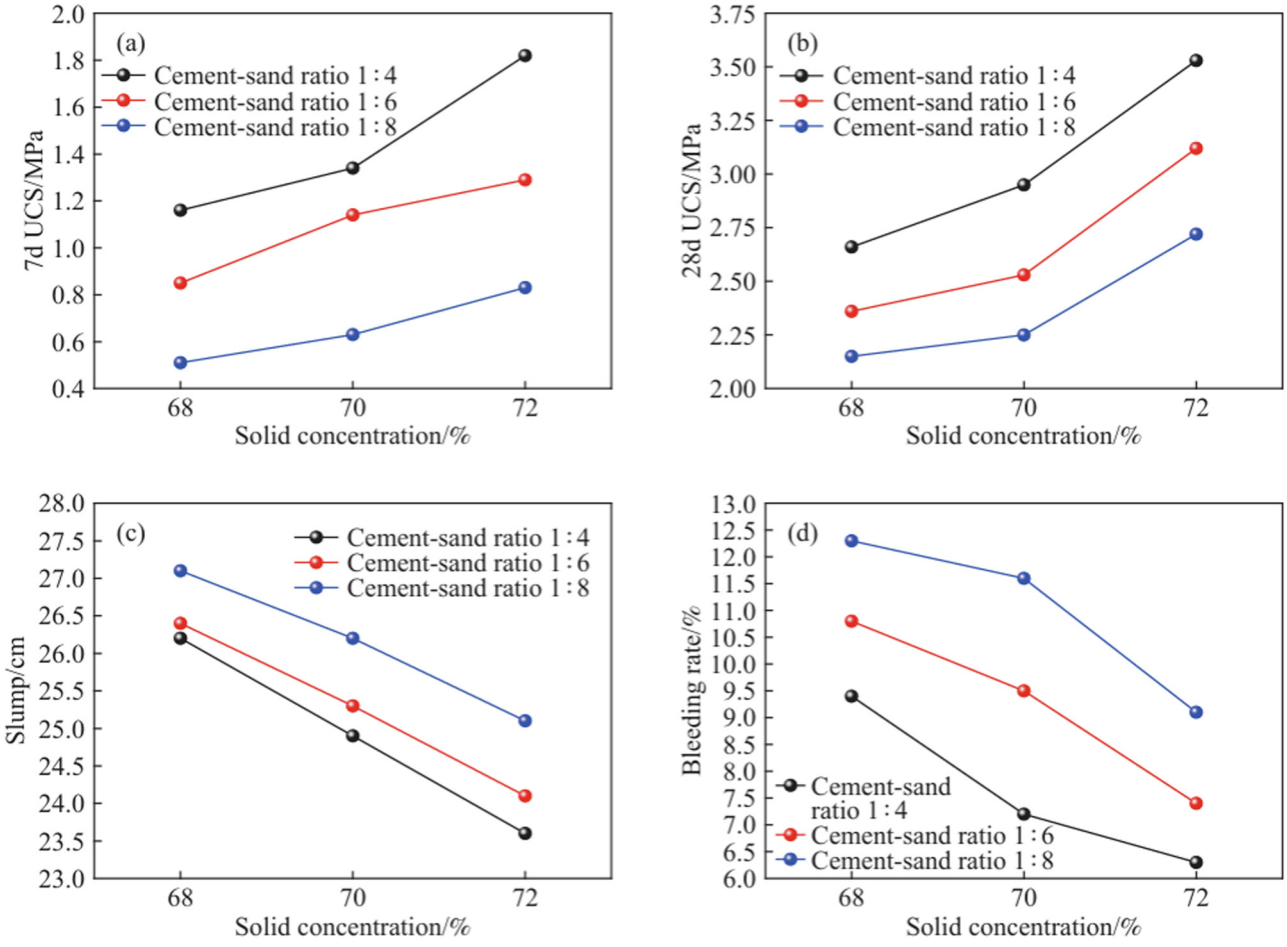

Figure 8: Effect of the solid phase mass fraction on the characteristics of the slurry: (a) strength after 7 days; (b) strength after 21 days; (c) collapse; and (d) rate of water discharge.

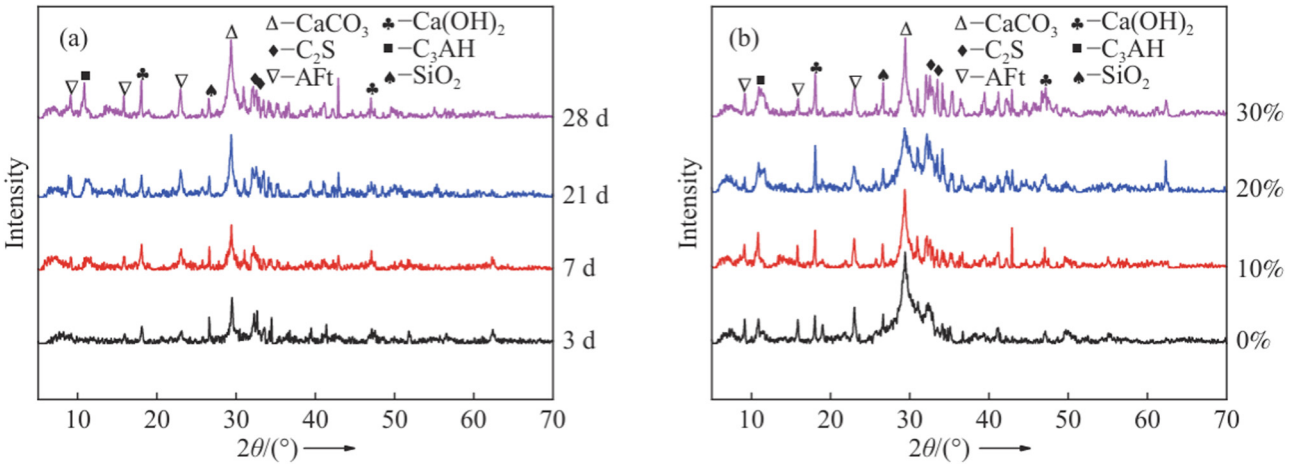

Figure 9: X-ray diffraction study of the hydration product: (a) hydration products at various ages of curing and (b) hydration products on day 21 with varying dosages of steel slag.

The slurry mix with a 1:6 cement/sand ratio shows a lower cost and relatively lower compressive strength on day 7, suggesting it may be suitable for applications where cost is a priority but strength requirements are less stringent.

4.5 Choosing the filling material ratio

The proportioning of filling materials in the 302 operating face in the mining area of Tsahasu Coal Mine was made

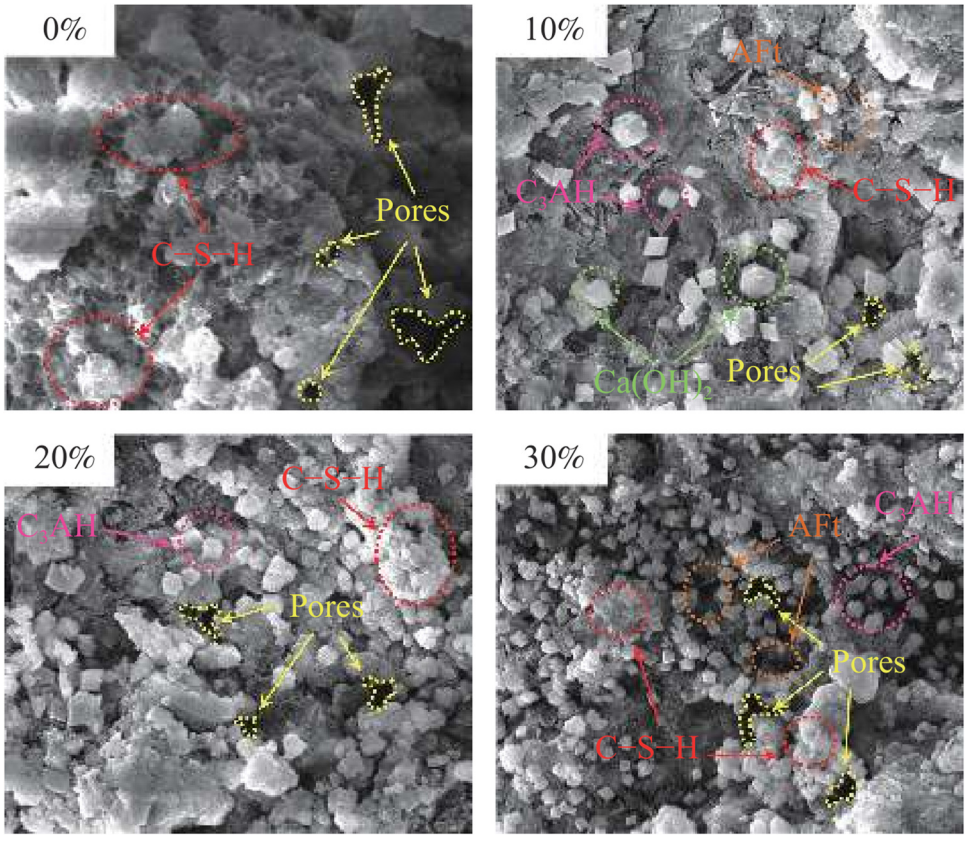

Figure 10: Microscopic appearance of the hydration products after 21 days in specimens that received varying amounts of steel slag.

possible by the test and result analysis mentioned above. According to the test results, the strength is comparatively low when the mass fraction of solids is 75%. However, when the mass fraction of solids is 80–81%, the strength is greater, but the slurry's fluidity is poor, which can easily cause blockage during the self-slipping transportation process. For this reason, the mass fraction of solids is kept at 75–78%. The operating face of the 302 Chahasu Coal Mine stipulates that the first stage filler's strength must not be less than 4.5 MPa throughout the filling operation, and the fourth-stage filler's strength must not be less than 2.5 MPa. The cement content is decreased, and the fly ash content is increased based on the starting proportion in order to lower the cost of cement and increase the amount of fly ash used [19–21].

4.6 Mechanism of hydration

It is evident from the earlier investigation that the strength of the filled cementitious material is significantly impacted by the dosage of steel slag. The net slurry specimens were created using the ideal ratio of exciters (12% clinker, 4% FGD gypsum, and 1% manganese nitrate) and varying dosages of steel slag, specifically 0, 10, 20, and 30%. The observation specimens were then created by keeping the net slurry specimens until various ages, and the hydration products of the net slurry specimens were examined using XRD and SEM. The hydration products of net slurry specimens with varying dosages of steel slag were examined using XRD and SEM. Figures 9 and 10 show the XRD and SEM images of the cementitious materials made from steel slag's hydration products, respectively. After 7 days of hydration, a thorough analysis reveals that the hydration products of the composite cementitious material – calcium alumina, hydrated tricalcium aluminate, $Ca(OH)_2$, and $CaCO_3$ – have clear diffraction peaks. The convex packets in the 20–35° range are typically thought to be made of the C–S–H gel with an amorphous non-crystalline structure. Calomel, $Ca(OH)_2$, and tricalcium aluminate rods and needles are used to fill the spaces in the networked C–S–H gels. A denser structure and greater strength were achieved as the maintenance time increased. It is evident that as age increased, the intensity of the $Ca(OH)_2$ and AFt diffraction peaks increased steadily. This is because the hydration of steel slag and clinker produced $Ca(OH)_2$, and the alkaline environment created by $Ca(OH)_2$ promoted the hydrolysis of slag to produce C–S–H gels, which in turn reacted with SiO_2 to produce calcium alunite. $Ca(OH)_2$ creates an alkaline environment that promotes slag hydrolysis to create C–S–H gels, which then combine with SiO_2 to create calcium alumina. The diffraction peaks of gypsum are not visible because the system's mannite and gypsum have completely reacted. The specimen developed many pores and a looser structure as the dosage of steel slag increased, causing a decrease in C–S–H and an increase in (hexagonal) platelets of calcium hydroxide and other hydration products.

5 Conclusion

The research backdrop of this study is the Inner Mongolia Chahasu coal mine. A unique cementitious filling material based on gangue, fly ash, and cement was developed in response to the need for cost-effective and efficient cementitious filling materials for coal mine mining and filling. Following a comprehensive analysis to optimize the ratio and the performance-affecting elements, the following conclusions were drawn: The particle size level of the filler body has a major effect on its strength and mobility. By adjusting the particle size grading coefficient, the optimal gangue grading coefficient is found to be $n = 0.5$. Under these conditions, the filling material shows good mechanical and fluid qualities, which can be used as a guide when designing the base percentage of the filling material. The primary factors influencing the filler's compressive strength were the cement mass fraction and solid mass fraction, according to the Box–Behnken experimental design and response surface analysis. Fly ash significantly boosted the filler's contribution to the late (21 days) strength, whereas the cement content largely controlled the early (3 days) strength. The interaction between fly ash and cement is crucial for optimizing performance. Through model optimization, the optimal ratio was discovered, significantly increasing the utilization of fly ash while reducing the cement quantity. The compressive strengths on days 3, 7, and 21 of the optimized filling body met the technical requirements of the coal mine filling and mining processes, respectively, and a balance between strength and fluidity was achieved.

Funding information: This study was supported by the Liaoning Province Science and Technology Plan Joint Program (Applied Basic Research Project) in 2023 under Grant No. 2023JH2/101700006.

Author contribution: All authors have accepted responsibility for the entire content of this manuscript and approved its submission.

Conflict of interest: Authors state no conflict of interest.

Data availability statement: The datasets generated during and/or analyzed during the current study are available from the corresponding author on reasonable request.

References

[1] Hong ZJ, Li ZH, Du F, Xu L, Zhu C. Experimental investigation of the mechanical properties and large-volume laboratory test of a novel filling material in mining engineering. Geomech Geophys Geo-Energy Geo-Resour. 2023;9(1):46.

[2] Feng J, Zhang Z, Guan W, Wang W, Xu X, Song Y, et al. Review of the backfill materials in Chinese underground coal mining. Minerals. 2023;13(4):473.

[3] Wang H, Chen D, Guo R, Tian J, Li B. A preliminary study on the improvement of gangue/tailing cemented fill by bentonite: Flow properties, mechanical properties and permeability. Materials. 2023;16(20):6802.

[4] Zhou Y, Wang C, Liao C, Wang J, Zhang B. Study on the mining effect and optimal design of longwall full mining with paste partial filling. Minerals. 2024;14(3):264.

[5] Wu A, Wang Y, Ruan ZE, Xiao B, Wang J, Wang L. Key theory and technology of cemented paste backfill for green mining of metal mines. Green Smart Min Eng. 2024;1(1):27–39.

[6] Bo L, Yang S, Liu Y, Zhang Z, Wang Y, Wang Y. Coal mine solid waste backfill process in China: current status and challenges. Sustainability. 2023;15(18):13489.

[7] Shi P, Zhang Y, Yan H, Zhang J, Gao D, Wang W. Evaluation of rheological and mechanical performance of gangue-based cemented backfill material: a novel hybrid machine learning approach. Environ Sci Pollut Res. 2023;30(19):55699–715.

[8] Zhang Z, Ding Q, Feng G, Qi T, Guo Y, Wang Y, et al. A novel economic benefit calculation modeling applying to coal mining. Environ Dev Sustainability. 2024;26(6):15307–31.

[9] Tian M, Chen S, Han L, Xiao H. Development and application of novel high-efficiency composite ultrafine cement grouts for roadway in fractured surrounding rocks. Deep Undergr Sci Eng. 2024;3(1):53–69.

[10] Gao B, Cao S, Yilmaz E. Effect of content and length of polypropylene fibers on strength and microstructure of cementitious tailings-waste rock fill. Minerals. 2023;13(2):142.

[11] Jin J, Chen Y, Li M, Liu T, Qin Z, Liu Q, et al. Preparation of self-consolidating cemented backfill with tailings and alkali activated slurry: Performance evaluation and environmental impact. Constr Build Mater. 2024;438:137088.

[12] Jiang TT, Cao S, Yilmaz E. Microstructure evolution and mechanical behavior of foamed cement-based tail backfills under varying fiber types and concentrations. Environ Sci Pollut Res. 2024;31(39):52181–97.

[13] Karadeniz KE, Guner D, Sherizadeh T. Failure analysis of abutment-loaded underground coal mine stoppings during explosion. Int J Geomech. 2024;24(6):04024100.

[14] Wang K. The construction of fuzzy prediction model of stock price rise and fall based on machine learning technology. J Comb Math Comb Comput. 2024;120:125–36.

[15] Ngo I, Ma L, Zhai J, Wang Y. Enhancing fly ash utilization in backfill materials treated with CO2 carbonation under ambient conditions. Int J Min Sci Technol. 2023;33(3):323–37.

[16] Jiliang X, Yanxia Z, Xia S. Preparation of TiO_2 graphene oxide composites and its application in coking wastewater treatment. Mari Pap Corrugado. 2024;2024(1):59–68.

[17] Yadav AK, Mishra S, Mishra DP. A detailed review study on utilization of mine and industrial wastes for backfill strengthening. Arab J Geosci. 2024;17(4):121.

[18] Ji H, Feng Y, Li H, Xin Y, Li J, Zhang D, et al. Pore-fractal-permeability model and its experimental analysis of construction waste filling body with high fine-particle content. Environ Earth Sci. 2024;83(12):365.

[19] Mohamed AO, El GM. A novel polymerized sulfur concrete for underground hydrogen storage in lined rock caverns. Sustainability (2071-1050). 2024;16(19):8595.

[20] Wei Z. Research on the key technology of high-performance nanomaterials for the enhancement of mechanical properties in modern industry. Mari Pap Corrugado. 2024;2024(1):48–56.

[21] Karadeniz KE, Nowak S, Guner D, Sherizadeh T. Dynamic response analysis of a reinforced concrete structure in underground coal mine environment with various strata conditions. Min Metall Explor. 2023;40(2):563–81.